

A planar parallel 3-DOF cable-driven haptic interface

Clément Gosselin
Department of Mechanical Engineering
Université Laval
Québec, Qc, Canada
gosselin@gmc.ulaval.ca

Régis Poulin and Denis Laurendeau
Department of Electrical Engineering
Université Laval
Québec, Qc, Canada
laurend@gel.ulaval.ca

ABSTRACT

In this paper, a cable-driven planar parallel haptic interface is presented. First, the velocity equations are derived and the forces in the cables are obtained by the principle of virtual work. Then, an analysis of the wrench-closure workspace is performed and a geometric arrangement of the cables is proposed. Control issues are then discussed and a control scheme is presented. The calibration of the attachment points is also discussed. Finally, the prototype is described and experimental results are provided.

Keywords: haptic interface, parallel mechanism, cable-driven mechanism, planar mechanism.

1. INTRODUCTION

Cable-driven parallel mechanisms have attracted the attention of several researchers over the past decades. The main advantages of this type of mechanism are large motion ranges, low inertia, low cost and robustness in case of interference [1]. Cable-driven parallel mechanisms have the potential to overcome several of the drawbacks of conventional mechanisms. Among others, they can produce large accelerations over a large workspace. Also, they have a small inertia. These advantages lead to a broad variety of potential applications. Hence, several groups of researchers have been working on cable-driven robots. For instance, cable-driven mechanisms have been studied in the context of applications such as a virtual sports machine based on a wire-driven system [2], a planar cable-suspended haptic interface [3], a high-speed manipulator using parallel wire-driven robots [4] and an air vehicle simulator [5]. In [6], it was proposed to use two cable-driven parallel mechanisms sharing a common workspace to design a locomotion interface. The concept is illustrated in Fig. 1. In this concept, the user's feet are attached to two moving platforms that are controlled using cables. Since the motion of a cable-driven mechanism involves low inertia, large accelerations can be produced, thereby allowing an accurate reproduction of the majority of sensations felt during natural walking on uneven terrains, stairs, sandy ground, etc. Also, the cable-driven mechanisms have a large workspace and a high bandwidth, which are ideal for a locomotion interface. However, cable mechanisms also have some drawbacks, including the unilaterality of the cables which leads to the necessity of having $n + 1$ cables to suitably constrain n degrees of freedom (DOFs).

This paper aims at providing an experimental validation of the concept underlying the locomotion interface based on cable-driven parallel mechanisms. In order to simplify the initial ex-

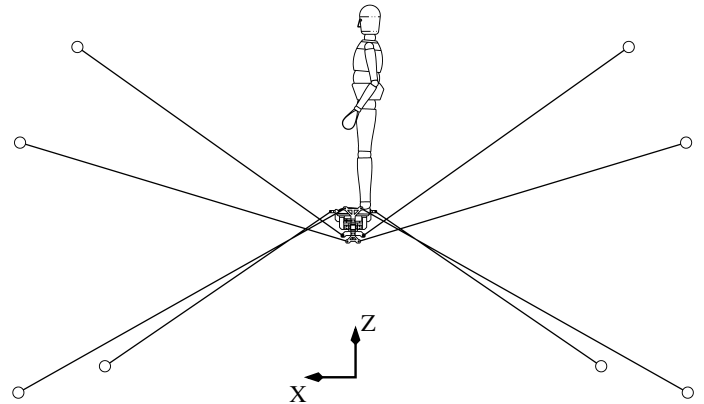


Figure 1: Concept of locomotion interface based on cable-driven parallel mechanisms.

perimental work, a planar 3-DOF architecture of mechanism is chosen, as illustrated schematically in Fig. 2. Moreover, in order to limit the forces involved, the platform of the prototype of haptic interface is manipulated with the hands. Although the 3-DOF cable-driven parallel mechanism developed in this work is mainly intended as a proof of concept of the locomotion simulator, it can also be considered on its own merits as a potential planar 3-DOF haptic interface.

The rest of this paper is structured as follows: Section 2 presents the kinematic model of the mechanism. Section 3 introduces the dynamic model and presents the equations used to compute the forces in the mechanism. Section 4 determines the wrench-closure workspace of the mechanism and shows the workspace of the mechanism. Section 5 presents the control algorithm used for the prototype, the latter being described in Section 6. Finally, the kinematic calibration of the prototype is discussed in Section 7 and a description of the experiments performed with the mechanism is provided in Section 8.

2. KINEMATIC MODELLING

Geometric Model

Consider a rigid body — the platform to be manipulated by the user of the haptic interface — moving in a plane and constrained by n cables attached to the platform and to actuated reels located on the fixed base. The i th point of attachment on the platform is noted V_i while the corresponding attachment point on the base is noted P_i . The position vector of point P_i is defined by vector \mathbf{p}_i expressed in the fixed reference frame $O - XY$, attached to the

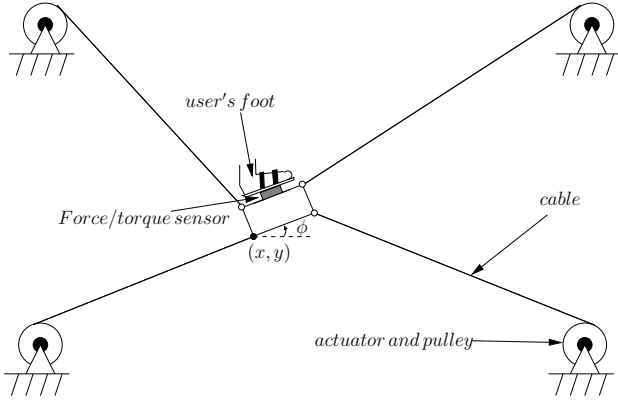


Figure 2: Planar three-degree-of-freedom cable-driven parallel mechanism.

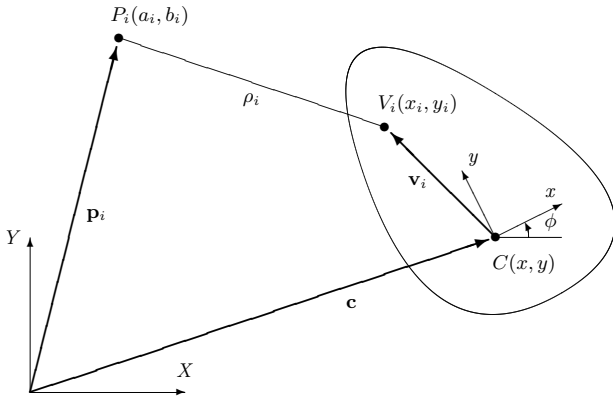


Figure 3: Kinematic model of the i th cable of the mechanism.

base, whereas the position vector of point V_i is defined by vector \mathbf{v}_i expressed in the mobile reference frame $C - xy$, attached to the platform and having its origin C at the centre of mass of the end-effector. The position of point C in the fixed frame is defined by vector \mathbf{c} , while the orientation of the moving frame relative to the fixed frame is given by angle ϕ (Fig. 3). Finally, vector ρ_i is defined as the vector connecting point P_i to point V_i and hence one has

$$\rho_i = \mathbf{c} + \mathbf{Q}\mathbf{v}_i - \mathbf{p}_i \quad (1)$$

where \mathbf{Q} is the rotation matrix from the fixed frame to the moving frame, written as

$$\mathbf{Q} = \begin{bmatrix} \cos \phi & -\sin \phi \\ \sin \phi & \cos \phi \end{bmatrix}. \quad (2)$$

Velocity Equations

Taking the norm of both sides of eq.(1) one obtains:

$$\begin{aligned} \rho_i^2 &= (\mathbf{c} + \mathbf{Q}\mathbf{v}_i - \mathbf{p}_i)^T (\mathbf{c} + \mathbf{Q}\mathbf{v}_i - \mathbf{p}_i), \\ \dot{\rho}_i^2 &= \mathbf{c}^T \dot{\mathbf{c}} + 2\mathbf{c}^T \mathbf{Q}\dot{\mathbf{v}}_i - 2\mathbf{c}^T \dot{\mathbf{p}}_i + \mathbf{v}_i^T \dot{\mathbf{v}}_i \\ &\quad - 2\mathbf{p}_i^T \mathbf{Q}\dot{\mathbf{v}}_i + \mathbf{p}_i^T \dot{\mathbf{p}}_i \end{aligned} \quad (3)$$

where ρ_i^2 stands for the square of the norm of vector ρ_i . Differentiating eq.(3) with respect to time and dividing by 2 throughout leads to

$$\rho_i \dot{\rho}_i = \mathbf{c}^T \dot{\mathbf{c}} + (\mathbf{Q}\mathbf{v}_i)^T \dot{\mathbf{c}} + \mathbf{c}^T \mathbf{Q}\dot{\mathbf{v}}_i - \mathbf{p}_i^T \dot{\mathbf{c}} - \mathbf{p}_i^T \mathbf{Q}\dot{\mathbf{v}}_i$$

with

$$\dot{\mathbf{Q}} = \dot{\phi} \mathbf{E} \mathbf{Q}, \quad \mathbf{E} = \begin{bmatrix} 0 & -1 \\ 1 & 0 \end{bmatrix},$$

and thus

$$\rho_i \dot{\rho}_i = (\mathbf{c} + \mathbf{Q}\mathbf{v}_i - \mathbf{p}_i)^T \dot{\mathbf{c}} + (\mathbf{c} - \mathbf{p}_i)^T \mathbf{E} \mathbf{Q} \mathbf{v}_i \dot{\phi}. \quad (4)$$

The velocity equations can therefore be written in matrix form as

$$\mathbf{A} \dot{\boldsymbol{\rho}} = \mathbf{B} \mathbf{t} \quad (5)$$

where vectors $\dot{\boldsymbol{\rho}}$ and \mathbf{t} are defined as

$$\dot{\boldsymbol{\rho}} = [\dot{\rho}_1 \quad \dot{\rho}_2 \quad \cdots \quad \dot{\rho}_n]^T, \quad (6)$$

$$\mathbf{t} = [\dot{x} \quad \dot{y} \quad \dot{\phi}]^T, \quad (7)$$

where matrix \mathbf{A} is a diagonal matrix whose i th diagonal entry is ρ_i , namely

$$\mathbf{A} = \begin{bmatrix} \rho_1 & 0 & 0 \\ 0 & \rho_2 & 0 \\ & & \ddots \\ 0 & 0 & \rho_n \end{bmatrix} \quad (8)$$

and where matrix \mathbf{B} is defined as

$$\mathbf{B} = \begin{bmatrix} \mathbf{b}_1^T \\ \vdots \\ \mathbf{b}_n^T \end{bmatrix} \quad (9)$$

with

$$\mathbf{b}_i^T = \left[(\mathbf{c} + \mathbf{Q}\mathbf{v}_i - \mathbf{p}_i)^T \quad ((\mathbf{c} - \mathbf{p}_i)^T \mathbf{E} \mathbf{Q} \mathbf{v}_i) \right]. \quad (10)$$

3. DYNAMIC MODELLING

From the principle of virtual work, one can write

$$-\mathbf{f}^T \delta \boldsymbol{\rho} = \mathbf{e}^T \delta \mathbf{x} \quad (11)$$

with

$$\begin{aligned} \mathbf{f}^T &= [f_1 \quad f_2 \quad \cdots \quad f_n] \\ \mathbf{e}^T &= [F_x \quad F_y \quad \tau] \\ &= [(m\ddot{x} - r_x) \quad (m(\ddot{y} + g) - r_y) \quad (I\ddot{\phi} - r_\phi)] \end{aligned}$$

where f_i is the tensile force in cable i while F_x , F_y , and τ are the forces and torques applied by the cables to the end-effector. $\delta \boldsymbol{\rho}$ and $\delta \mathbf{x}$ are respectively the virtual changes in the length of the cables and the virtual generalized displacement of the end-effector. m and I are respectively the mass and the moment of inertia (about the centre of mass) of the end-effector and the external wrench applied by the user to the platform, noted \mathbf{r} is given by:

$$\mathbf{r} = [r_x \quad r_y \quad r_\phi]^T \quad (12)$$

where r_x , r_y and r_ϕ are respectively the force component in x , the force component in y and the torque. In the above, it is assumed that the xy plane is a vertical plane and that gravity is acting in the negative direction of the y axis.

From eq.(5), we have

$$\delta \boldsymbol{\rho} = \mathbf{A}^{-1} \mathbf{B} \delta \mathbf{x}. \quad (13)$$

Substituting in eq.(11), we obtain

$$-\mathbf{f}^T \mathbf{A}^{-1} \mathbf{B} \delta \mathbf{x} = \mathbf{e}^T \delta \mathbf{x}. \quad (14)$$

Since the latter equation must be valid for any Cartesian virtual displacement $\delta \mathbf{x}$, one finally has

$$\mathbf{W}\mathbf{f} = \mathbf{e} \quad (15)$$

where

$$\mathbf{W} = -\mathbf{B}^T \mathbf{A}^{-T}. \quad (16)$$

Equation (15) relates the forces in the cables, \mathbf{f} , to the dynamic conditions and external forces and torques on the platform, all contained in vector \mathbf{e} .

In the application considered here, i.e., in the context of a haptic device, the platform must be fully constrained in order to be capable of applying arbitrary forces and torques to the user. Therefore, given the unilaterality of the forces in the cables, the number of cables must be larger than three. Hence, matrix \mathbf{W} has more columns than rows and the linear system of eq.(15) generally admits infinitely many solutions. The classical minimum norm solution of eq.(15) cannot guarantee that all force components (cable tensions) are positive. The problem to be solved can rather be written as

$$\min \mathbf{f}^T \mathbf{f} \quad \text{s.t.} \quad \mathbf{W}\mathbf{f} = \mathbf{e} \quad \text{and} \quad f_i \geq 0, \forall i \quad (17)$$

Solving this problem is achieved through the use of quadratic programming [7, 8]. This method allows the determination of the minimum-norm vector of forces in the cables — if it exists — while satisfying a set of equality constraints (equilibrium equations) and a set of inequality constraints (cables in tension).

4. WORKSPACE

In [9], a method was proposed to determine the wrench-closure workspace of cable-driven planar parallel mechanisms. The wrench-closure workspace is defined as the set of configurations (poses) of the platform for which the latter can resist any external wrench while maintaining the cables in tension. Within this workspace, the mechanism is fully constrained, can produce external forces and torques of arbitrary direction and magnitude and is singularity-free. Therefore, the determination of the wrench-closure workspace is an important criterion in the design of a cable-driven parallel mechanism.

It was shown in [9] that the wrench-closure workspace of a planar cable-driven parallel mechanism is a bounded open set whose boundary can be described by portions of singularity curves of sub-mechanisms obtained by keeping only three of the cables. An algorithm was also proposed in order to automate the determination of the wrench-closure workspace.

For purposes of simplicity and in order to limit possible mechanical interferences, it was chosen here to use only four cables — the minimum possible number — and to attach them by pairs on the moving platform. Moreover, the attachment points on the base are located on the vertices of a rectangle. This arrangement of the cables simplifies the determination of the wrench-closure workspace because the lines associated with the cables intersect by pairs at the platform attachment points. Additionally, the following requirements were used for the usable workspace: the workspace should be a rectangle measuring $1m$ in the x direction and $30cm$ in the y direction. Within this rectangle, the orientation of the moving platform can be varied from -45° and 45° , for any position.

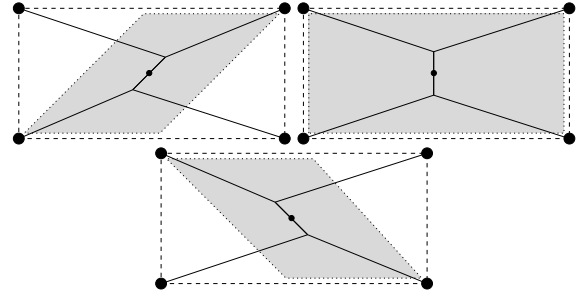


Figure 4: Wrench-closure workspace for 3 different orientations of the platform.

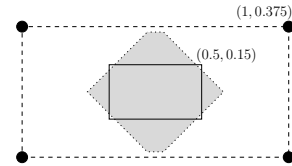


Figure 5: Wrench-closure workspace covering the desired range of orientations.

Given the simplified architecture described above, it is rather easy to determine the wrench-closure workspace for a given orientation of the moving platform. This is illustrated in Fig. 4, where the wrench-closure workspace is shown for orientations of the platform of -45° , 0° and 45° . Therefore, the wrench-closure workspace covering the complete required range of rotation can be determined as shown in Fig. 5. As a result, it can be seen that for a platform having a length of $10cm$, choosing the attachment points on the vertices of a rectangle of $2m$ by $75cm$ provides the desired workspace.

5. CONTROL

The moving platform of the mechanism is equipped with a force/torque sensor that provides a measure of the interaction wrench between the user and the platform. However, with the current prototype, no direct measure of the forces in the cables is available. Therefore, the prototype is controlled using a position control algorithm in which the wrench measured by the force/torque sensor mounted on the platform is used to infer the intentions of the user and determine corresponding prescribed platform poses. In other words, the prescribed pose of the platform is updated based on the wrench measured by the force/torque sensor. The prescribed pose of the platform is incremented in the direction of the measured wrench with an incremental magnitude proportional to the measured wrench. The pose of the platform, noted \mathbf{s} , is represented by a vector with three components defined as:

$$\mathbf{s} = [\mathbf{c}^T \quad \phi]^T. \quad (18)$$

Assuming that the acceleration of the platform is constant over a given time step, the displacement (change of pose) of the platform over a time step can then be written as:

$$\mathbf{s}_{i+1} = \mathbf{s}_i + T\dot{\mathbf{s}}_i + \frac{1}{2}T^2\ddot{\mathbf{s}}_i \quad (19)$$

where \mathbf{s}_i is the pose of the platform at the beginning of time step i , $\dot{\mathbf{s}}_i$ is the time derivative of the pose of the platform at the beginning of time step i , $\ddot{\mathbf{s}}_i$ is the (constant) acceleration of the

platform during time step i and T is the duration of one time step (period), i.e.,

$$T = \frac{1}{\nu} \quad (20)$$

where ν is the control frequency (servo rate).

For a given acceleration vector \ddot{s}_i , eq.(19) allows the computation of the displacement (change of pose) of the platform which can then be used as a prescribed pose in the control loop. The acceleration vector to be used in eq.(19) can be determined using the dynamic model of the mechanism. Indeed, the generalized mass matrix of the platform is written as

$$\mathbf{M} = \begin{bmatrix} m & 0 & 0 \\ 0 & m & 0 \\ 0 & 0 & I \end{bmatrix} \quad (21)$$

and hence the dynamic model of the platform considered as a free-floating body can be written as

$$\mathbf{r} = \mathbf{M}\ddot{\mathbf{s}}_i \quad (22)$$

where it is recalled that \mathbf{r} is the external wrench applied to the platform by the user and measured by the force/torque sensor. In practice, in order to improve the sensitivity of the platform, a friction force is added to eq.(22). Finally, the acceleration of the platform is determined using:

$$\ddot{\mathbf{s}}_i = \mathbf{M}^{-1}(\mathbf{r} + \mathbf{r}_f) \quad (23)$$

where \mathbf{r}_f is an additional term used to account for viscous friction forces. This term is adjusted experimentally.

In the controller, eq.(23) is first used to compute the acceleration vector $\ddot{\mathbf{s}}_i$. Then, this vector is substituted into eq.(19) to compute the new prescribed pose of the platform, which is then controlled using a standard pose feedback loop based on a PID controller.

The above scheme is used as long as the platform is not interfering with virtual obstacles. When interferences are detected, the corresponding motions — motions that would bring the platform inside the virtual obstacles — are inhibited. For instance, if the platform is making contact with a virtual wall, motion towards the wall is inhibited and the prescribed pose, computed using eq.(19) is modified accordingly. This scheme allows the user to make the platform *slide* along virtual obstacles without interfering with them.

6. PROTOTYPE

A prototype of a 3-DOF cable-driven planar haptic interface was built to demonstrate the feasibility of the concept and to test the effectiveness of the proposed control scheme. Photographs of the prototype are shown in Fig. 6. The prototype is driven by four cables attached to the platform by pairs. The position of the attachment points is as described in Section 4. The mechanism is moving on a vertical plane. A force/torque sensor (shown on the second photograph) is mounted on the platform and is used to determine the interaction wrench that the user is applying to the platform. The actuators are DC motors with encoders driving spools on which the steel cables are wound. The complete set-up is shown in Fig. 7.

7. CALIBRATION

In order to ensure a proper performance of the mechanism, the position coordinates of the attachment points of the cables on the

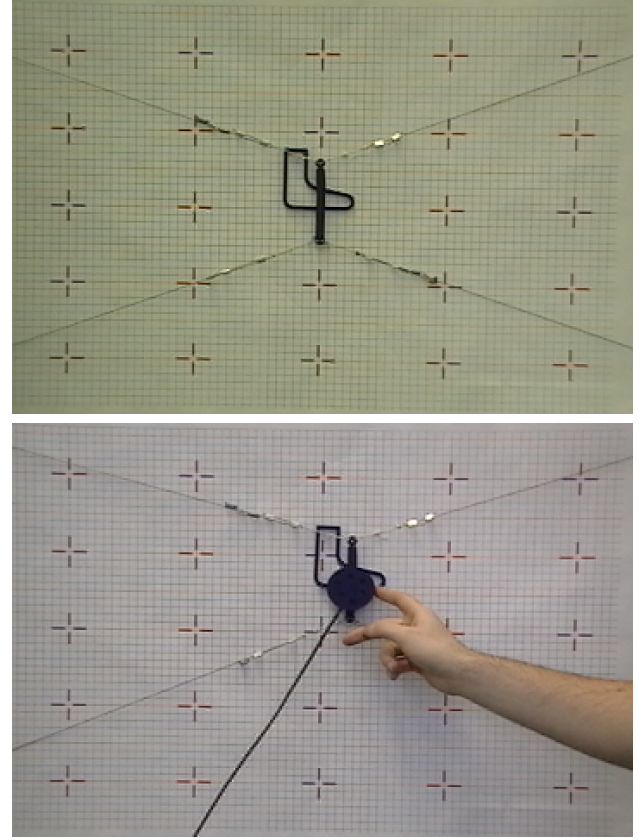


Figure 6: Photographs of the prototype of the 3-DOF cable-driven planar haptic interface.

fixed frame and on the platform must be calibrated. Indeed, it is apparent from eq.(1) that errors on these position coordinates will lead to errors on the cable extensions which may lead to poor position control performances.

A simple and effective calibration procedure was used on the prototype developed in this work. As shown in Fig. 6, a calibration grid was pasted on the surface of the workspace. This grid was used as a reference for the Cartesian pose of the platform. The calibration procedure consisted in bringing the platform to a set of m chosen poses and measuring the corresponding cable lengths using the motor encoders. A calibration performance index was then defined as follows:

$$\eta = \sum_{i=1}^m \sum_{j=1}^4 \left[(\mathbf{c}_i + \mathbf{Q}_i \mathbf{v}_j - \mathbf{p}_j)^T (\mathbf{c}_i + \mathbf{Q}_i \mathbf{v}_j - \mathbf{p}_j) - \rho_{ji}^2 \right] \quad (24)$$

where \mathbf{c}_i and \mathbf{Q}_i describe the pose of the i th measurement configuration (pose), \mathbf{v}_j and \mathbf{p}_j are the position coordinates to be calibrated and ρ_{ji} is the measured length of the j th cable in the i th measurement configuration. The calibration then consists in solving the following optimization problem:

$$\min_{\mathbf{v}_i, \mathbf{p}_i, i=1, \dots, 4} \eta^2. \quad (25)$$

This optimization was solved numerically using a nonlinear least squares technique. Finally, upon convergence, calibrated values for $\mathbf{v}_i, \mathbf{p}_i, i = 1, \dots, 4$ were obtained.

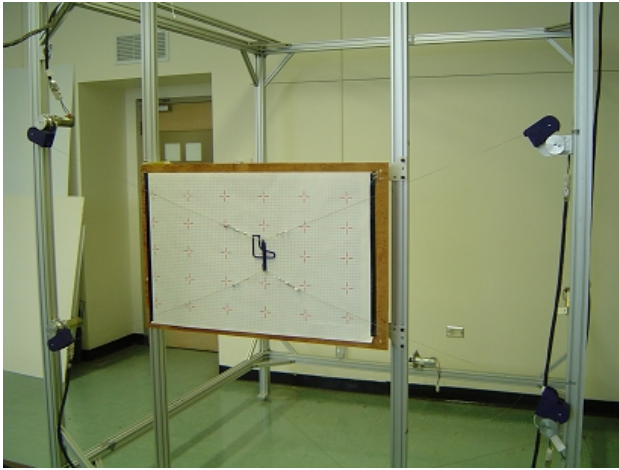


Figure 7: Photograph of the complete set-up.

8. EXPERIMENTAL VALIDATION

Experiments were performed on the prototype described above. The control scheme was implemented on a RT-LAB based real-time controller. First, the position control of the platform was tested — without using the force/torque sensor. The position was observed to be very stable and the platform was stiff when resisting to external forces and torques applied to the platform.

Then, the position control scheme was used to perform prescribed trajectories with the platform. A trajectory planning algorithm based on fifth order polynomials [10] was used to generate smooth trajectories. A visual inspection of the trajectories reveals that the platform can be positioned — and oriented — precisely and that the motion between given points is very smooth.

Finally, the force/torque sensor was mounted on the platform and the control scheme described in Section 5 was implemented. It can be verified that the platform can be moved arbitrarily by a user by exerting very little force on the force/torque sensor. In the locomotion interface, this property is very important in order to allow the user to move his/her feet in free space. Then, virtual walls are defined in the controller (see Fig. 8) and it can be observed that the user can very well feel the virtual walls when moving the platform around. Sliding motions along the virtual walls are also possible. The apparent stiffness of the virtual walls is large, which is an important property for the locomotion interface in which the user should feel sharp contacts when putting his/her feet on the ground. A video demonstrating the experiments described in this section is available at [11].

9. CONCLUSION

A cable-driven planar parallel 3-DOF haptic interface was presented in this paper. This mechanism was developed as a basic proof of concept for a spatial locomotion interface. First, the velocity equations of cable-driven parallel mechanisms were derived and the principle of virtual work was used to determine the forces in the cables. Then, a geometric arrangement of the cables was proposed in order to ensure a sufficient wrench-closure workspace. Control issues were then addressed. The control of the prototype developed in this work is based on the use of the force/torque sensor to infer the intentions of the user and to calculate corresponding prescribed poses. At the lowest level, a

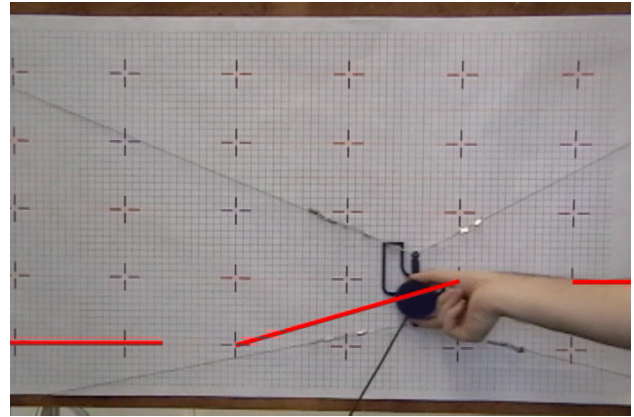


Figure 8: Prototype of the 3-DOF cable-driven planar haptic interface with virtual walls.

position control scheme is used. The calibration of the prototype was also performed using a nonlinear least squares approach in order to precisely determine the position of the attachment points of the cables on the base and on the platform. Finally, the prototype was tested experimentally and qualitative results were provided. The prototype presented in this paper demonstrated the feasibility of the use of a cable-driven parallel mechanism as a locomotion interface. The results of this paper are currently being extended to 6-DOF three-dimensional cable-driven mechanisms.

ACKNOWLEDGEMENTS

The authors would like to thank the Natural Sciences and Engineering Research Council of Canada (NSERC) as well as the Canada Research Chair Program (CRC) for their financial support. The help of Guillaume Barrette, Simon Perreault, Ian Tremblay and Boris Mayer St-Onge with some of the figures is also acknowledged.

REFERENCES

- [1] Landsberger, S.E. and Sheridan, T.B., 1993, "A Minimal, Minimal Linkage: The Tension-Compression Parallel Link Manipulator", *Robotics, Mechatronics and Manufacturing Systems*, pp. 81–88.
- [2] Kawamura, S., Ida, M., Wada, T., Wu, J.-L., 1995, "Development of A Virtual Sports Machine using A Wire Drive System: A Trial of Virtual Tennis", *IEEE: Proceedings of the International Conference on Intelligent Robots and Systems*, pp. 111–116.
- [3] Williams II, R. L., 1999, "Planar Cable-Suspended Haptic Interface: Design for Wrench Exertion", *Proceedings of the 1999 ASME Design Technical Conferences, 25th Design Automation Conference, DETC99/DAC-8639*, Las Vegas, United-States, September.
- [4] Kawamura, S., Kino, H., Won, C., 2000, "High-speed manipulation by using parallel wire-driven robots", *Robotica*, Vol. 18, No. 1, pp. 13–21.
- [5] Usher, K., Winstanley, G., Corke, P., Stauffacher, D., 2005, "Air Vehicle Simulator: an Application for a Cable Array Robot", *IEEE: Proceedings of the International Conference on Robotics and Automation (ICRA05)*, Barcelona, Spain, April, pp. 2253–2258.
- [6] Perreault, S. and Gosselin, C., 2007, "Cable-driven parallel mechanisms: application to a locomotion interface", *PROVOLUME 7 - NUMBER 3 - YEAR 2009* ISSN: 1690-4524

ceedings of the ASME Mechanisms and Robotics Conference, Las Vegas, Sept. 4–7.

- [7] Nahon, M., 1991, “Optimization of Force Distribution in Redundantly-Actuated Robotic Systems”, Ph.D. Thesis, McGill University, Montreal, Canada.
- [8] Goldfarb, D. and Idnani, A., 1983, “A Numerically Stable Dual Method for Solving Strictly Convex Quadratic Programs”, *Mathematical Programming*, Vol. 27, No. 1, pp. 1–33.
- [9] Gouttefarde, M., Gosselin, C. M., 2006, “Analysis of the Wrench-Closure Workspace of Planar Parallel Cable-Driven Mechanisms”, *IEEE Transactions on Robotics*, Vol. 22, No. 3, pp. 434–445.
- [10] Gosselin, C. and Hadj-Messaoud, A., 1993, “Automatic planning of smooth trajectories for pick-and-place operations”, *ASME Journal of Mechanical Design*, Vol. 115, No. 3, pp. 450–456.
- [11] http://robot.gmc.ulaval.ca/videos/cables/force/Simulateur_de_marche_Regis.mpg